Published by :
http://www.ijert.org

International Journal of Engineering Research & Technology (IJERT)
ISSN: 2278-0181
Vol. 13 Issue 08, August-2024

Kinematic Analysis of a Double-Layer Parallel Superimposed Mechanism

Zhiyong Meng
Tianjin University of Technology and Education
Tianjin China

***Abstract*: In order to make the parallel mechanism reach the level of the series mechanism in the working space, a new type of coupling mechanism is proposed, which is coupled in the form of the basic configuration of the parallel mechanism, and then the position positive solution of the double-layer parallel mechanism can be derived. Through the differential mapping relationship of the finite instantaneous spiral theory, the velocity of the mechanism is solved. Finally, through motion simulation, it is verified that the performance of the mechanism is consistent with the theoretical analysis.**

***Keywords*: double-layer parallel mechanism; finite instantaneous spiral theory; differential transformations; positive kinematics**

1. INTRODUCTION

Compared with the series mechanism, the parallel mechanism has many advantages such as high stiffness, large bearing capacity, good dynamic performance and high precision, but the disadvantages of the parallel mechanism in the working space are also obvious, so that the application in practice is still very limited, and the parallel machine tool, the parallel attitude adjustment platform and the multi-degree-of-freedom motion simulator are mainly concentrated at present. However, there is still a shortage of parallel mechanisms with large working spaces, especially those with rotational freedom. Therefore, the parallel mechanism with a large working space has high research value and broad application prospects. Li Qinchuan [3] replaced the mechanism with the equivalent motion pair according to the relationship between the moving platform and the fixed platform, and analyzed the research status and research direction of the two-shift and one-shift parallel mechanism by relevant scholars at home and abroad. Yulin Zhou [4] of Yanshan University proposed a workspace mapping method based on bias output, which changes the institutional workspace by changing the bias angle. Miseabadesu [5] expanded the working space by optimizing the scale parameters of the 3-UPU parallel mechanism and the 3-UPS&S parallel mechanism, and the effect was remarkable. Carol Miller [6] increased the working space of the paralleling mechanism by optimizing the position of the drive unit on the frame. United States scholar Rossheim Mark [7] proposed a variety of large workspace parallel mechanism configurations and applied them to robots. Zhang Yaojun et al. [8] optimized the scale of a class of three-translational degrees of freedom parallel mechanism to increase the working space. Tao Zongjie et al. [9] proposed an effective design method based on the influence of member interference on the working space, and verified it in the design of the 3-RRR parallel mechanism. Chen Jianghong [10] used the idea of virtual axis and used the diamond-shaped mechanism as a branch chain to reduce the limitation of rod length on the working space, which not only improved the performance of the working space, but also increased the longitudinal expansion ratio. Bai Zhifu [11] designed a composite spherical pair with three rotating pairs from the perspective of improving the spherical pair of the parallel mechanism, so as to increase the swing angle and then expand the attitude space of the parallel mechanism. Xu Dongguang [12] used the idea of function optimization to obtain the influence of changing the scale parameters on the working space of the 6-UPS parallel mechanism, and gave a solution.

In addition, a new mechanism formed by connecting another mechanism in series on the basis of a parallel mechanism is a hybrid mechanism [13], and this tandem method can also improve the working space. However, it is more difficult to study the hybrid mechanism, and for location analysis, the relationship between input and output is often difficult to determine, so there are multiple solutions, which makes the practicability of the mechanism lacking. The traditional spiral [14] method is often complex for velocity solving.

In order to make the parallel mechanism reach the level of the series mechanism in the working space, a new type of coupling connection mechanism is proposed [15]. This configuration uses a mechanical transmission mode to transmit force and motion between parallel mechanisms, and after the coupling of two parallel mechanisms, the motion characteristics similar to those of the series mechanism are realized, and the important performance of the working space is reached or even better than that of the series mechanism [16]. For the velocity solution, the finite instantaneous spiral theory is used to make the process

International Journal of Engineering Research & Technology (IJERT)
ISSN: 2278-0181
Vol. 13 Issue 08, August-2024

2. DOUBLE-LAYER PAR-ALLEL MECHANISM CONFI G-URATION

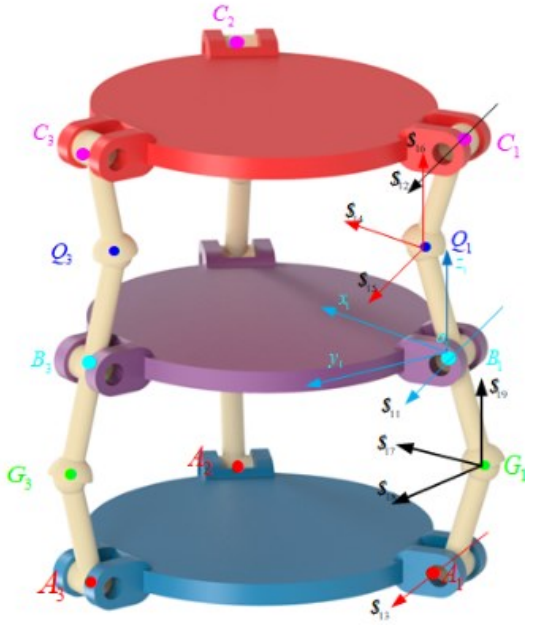

Figure 1 Mechanism Configuration

Although the double-layer parallel mechanism appears as a superposition of two 3-RSR parallel mechanisms, it can be considered as a 3-RSR parallel mechanism with three coplanar rotational constraints added at the shared linkage, due to the common linkage between the front and rear stages.

The difference between this mechanism and traditional double-layer parallel mechanisms lies in the fact that traditional parallel stacking requires two levels of actuation, which inevitably increases the self-weight of the mechanism and reduces its dynamic performance. By modifying the kinematic pairs at the end of the mechanism to create shared kinematic pairs, the upper and lower stages of the mechanism are connected through these kinematic pairs. The kinematic pairs accurately transmit the motion output of the upper parallel mechanism to the lower mechanism as the motion input of the lower parallel mechanism. This design requires only one set of actuators placed at the base platform, reducing the overall weight of the mechanism and enhancing its stability.

As shown in Figure 1, the origin of the branch coordinate system is selected at the center of the rotational pair of the middle platform. The Z axis is perpendicular to the middle platform and points towards the moving platform, the X axis points positively towards the center of the middle platform, and the Y axis direction is determined according to the right-hand rule. Due to the symmetry of the mechanism, points A, B, and C are all on the Z axis, and points G_1 and Q_1 are symmetric about the origin. Based on this, the coordinates of points A_1, C_1, G_1, Q_1 can be set as $(0 \quad 0 \quad -a)$, $(0 \quad 0 \quad -a)$, $(b \quad 0 \quad c)$ and $(-b \quad 0 \quad -c)$.

According to the directions of the screws in the figure 1, the motion screw system of this branch can be written as:

$$\begin{cases} \$_{11} = (0 \quad 1 \quad 0 \quad ; \quad 0 \quad 0 \quad 0) \\ \$_{12} = (0 \quad 1 \quad 0 \quad ; \quad -a \quad 0 \quad 0) \\ \$_{13} = (0 \quad 1 \quad 0 \quad ; \quad a \quad 0 \quad 0) \\ \$_{14} = (1 \quad 0 \quad 0 \quad ; \quad 0 \quad c \quad 0) \\ \$_{15} = (0 \quad 1 \quad 0 \quad ; \quad -c \quad 0 \quad b) \\ \$_{16} = (0 \quad 0 \quad 1 \quad ; \quad 0 \quad -b \quad 0) \\ \$_{17} = (1 \quad 0 \quad 0 \quad ; \quad 0 \quad -c \quad 0) \\ \$_{18} = (0 \quad 1 \quad 0 \quad ; \quad c \quad 0 \quad -b) \\ \$_{19} = (0 \quad 0 \quad 1 \quad ; \quad 0 \quad b \quad 0) \end{cases} \tag{1}$$

Since the rank of the aforementioned motion screw system is 6, the constraint screws can only be:

$$\$_1^r = (0 \quad 0 \quad 0 \quad ; \quad 0 \quad 0 \quad 0) \tag{2}$$

Therefore, the branch does not impose any constraints on the platform. Additionally, since the mechanism's three branches are of the same type, the moving platform should have 6 degrees of freedom. For a 3-RSR parallel mechanism, in non-singular configurations, the movement of the platform is determined when the inputs are specified, possessing three degrees of freedom: two rotational and one translational. The linkage in the middle layer functions as a single-degree-of-freedom transmission element, which does not increase the degrees of freedom. Consequently, the overall mechanism should also have 3 degrees of freedom.

International Journal of Engineering Research & Technology (IJERT)
ISSN: 2278-0181
Vol. 13 Issue 08, August-2024

3. DIRECT KINEMATIC ANALYSIS

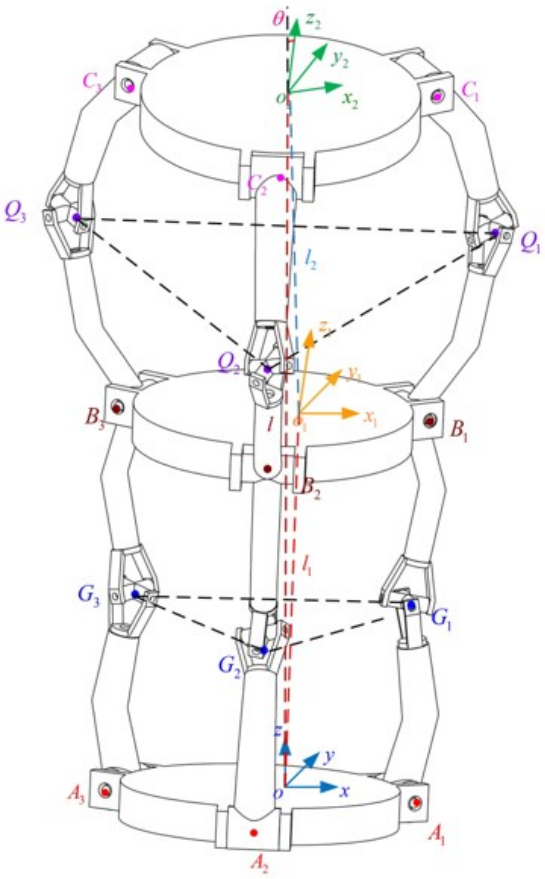

Figure 2 Schematic Diagram of the Mechanism

As shown in Figure 2, the mechanism is composed of three parts: the static platform, the moving platform, and the branches. The branches are distributed in a 360° circular arrangement. Each set of branches includes both active and passive links, where the active links are connected to the moving platform and the passive links are connected to the static platform.

Coordinate systems are established as follows: a fixed coordinate system $O-xyz$ on the static platform and a moving coordinate system $O_1-x_1y_1z_1$ on the moving platform. The origins O, O_1 and O_2 are the centers of the static and moving platforms, respectively. The x axis is aligned along vector $\boldsymbol{OA}_1$, the z axis is perpendicular to the static platform and points vertically upwards. The x_1 axis is aligned along vector $\boldsymbol{O_1B_1}$, the z_1 axis is perpendicular to the moving platform, the x_2 axis is aligned along vector $\boldsymbol{O_2B_2}$, and the z_2 axis is perpendicular to the moving platform. Define δ as the angle between the projection of the moving coordinate system's z_2 axis on the base plane and the positive direction of the fixed coordinate system's x axis. Let θ be the angle between the z_2 axis of the moving coordinate system and the z_2 axis of the fixed coordinate system. The distance between the centers of the moving and static platforms is l_i, and the distance from the platform center to the center of the rotational pair is R. All link lengths are L. Points G_1, G_2, and G_3 can be expressed in terms of the input angles β_1, β_2, and β_3.

$$G_1 = \begin{bmatrix} R - Lc\beta_1 \\ 0 \\ Ls\beta_1 \end{bmatrix} \quad (3)$$

$$G_2 = \begin{bmatrix} -\frac{1}{2}(R - Lc\beta_2) \\ \frac{\sqrt{3}}{2}(R - Lc\beta_2) \\ Ls\beta_2 \end{bmatrix} \quad (4)$$

$$G_3 = \begin{bmatrix} -\frac{1}{2}(R - Lc\beta_3) \\ \frac{\sqrt{3}}{2}(R - Lc\beta_2) \\ Ls\beta_3 \end{bmatrix} \quad (5)$$

International Journal of Engineering Research & Technology (IJERT)
ISSN: 2278-0181
Vol. 13 Issue 08, August-2024

The vectors $\boldsymbol{G_1G_2}$ and $\boldsymbol{G_1G_3}$ are further determined as follows:

$$\boldsymbol{G_1G_2} = \begin{bmatrix} -\frac{1}{2}(3R - 2Lc\beta_1 - Lc\beta_2) \\ \frac{\sqrt{3}}{2}(R - Lc\beta_2) \\ L(s\beta_2 - s\beta_1) \end{bmatrix} \quad (6)$$

$$\boldsymbol{G_1G_3} = \begin{bmatrix} -\frac{1}{2}(3R - 2Lc\beta_1 - Lc\beta_3) \\ -\frac{\sqrt{3}}{2}(R - Lc\beta_3) \\ L(s\beta_3 - s\beta_1) \end{bmatrix} \quad (7)$$

The cross product of the vectors $\boldsymbol{G_1G_2}$ and $\boldsymbol{G_1G_3}$ yields a vector that is normal to the plane $G_1G_2G_3$, with the direction pointing from the static platform to the moving platform. Using the coordinates of point G_1 and the normal vector, the point-normal form equation of the plane $G_1G_2G_3$ can be obtained. This allows for the calculation of the distance from point O to the plane $G_1G_2G_3$.

$$d = \frac{|-(m_1(R - Lc\beta_1) + pLs\beta_1)|}{\sqrt{m_1^2 + k_1^2 + p_1^2}} \quad (8)$$

Therefore, the solution parameters are:

$$l = OO_1 = 2d = \frac{2|-(m(R - Lc\beta_1) + pLs\beta_1)|}{\sqrt{m^2 + k^2 + p^2}} \quad (9)$$

$$\delta = \begin{cases} \arctan\frac{k}{m} (m \geq 0, k \geq 0) \\ \arctan\frac{k}{m} + \pi (m < 0) \\ \arctan\frac{k}{m} (m \geq 0, k < 0) \end{cases} \quad (10)$$

$$\theta = 2\varphi = 2\arctan\frac{\sqrt{m^2 + k^2}}{p} \quad (11)$$

Where

$$\sqrt{}$$

m=√3/2(RLsβ_3+RLsβ_2-2Rsβ_1-L^2 cβ_2 sβ_3-L^2 cβ_3 sβ_2 +Lcβ_2 sβ_1+Lcβ_3 sβ_1)

$\overline{k}$=1/2(3RLsβ_2-2L^2 cβ_1 sβ_2-L^2 cβ_3 sβ_2+Lcβ_3 sβ_1-3RLsβ_3 +2L^2 cβ_1 sβ_3+L^2 cβ_2 sβ_3-Lcβ_2 sβ_1))

$$p = \frac{\sqrt{3}}{4}(6R^2 - 4RLc\beta_3 - 2RLc\beta_1 - 4RLc\beta_2 + 3L^2c\beta_2c\beta_3)$$

The rotation matrix ${}^{O}\boldsymbol{R}_{O_1}$ representing the orientation of the moving coordinate system relative to the fixed coordinate system can be expressed as:

$${}^{O}\boldsymbol{R}_{O_1} = \begin{bmatrix} s\delta_1v\theta_1 + c\theta_1 & -s\delta_1c\delta_1v\theta_1 & c\delta_1s\theta_1 \\ -s\delta_1c\delta_1v\theta_1 & c^2\delta_1v\theta_1 + c\theta_1 & s\delta_1s\theta_1 \\ -c\delta_1s\theta_1 & -s\delta_1s\theta_1 & c\theta_1 \end{bmatrix} \quad (12)$$

$s\delta = \sin\delta, c\theta = \cos\theta, v\theta = 1 - \cos\delta$ $\varphi = \frac{\theta}{2}$ is the angle between the OO_2 axis of the moving coordinate system and the z axis of the fixed coordinate system.

The coordinates of Q_1, Q_2 and Q_3 relative to the fixed coordinate system O_1 are:

International Journal of Engineering Research & Technology (IJERT)
ISSN: 2278-0181
Vol. 13 Issue 08, August-2024

$$^{O_1}Q_1 = \begin{bmatrix} R - Lc\beta_1' \\ 0 \\ Ls\beta_1' \end{bmatrix} \quad (13)$$

$$^{O_1}Q_2 = \begin{bmatrix} -\frac{1}{2}(R - Lc\beta_2') \\ \frac{\sqrt{3}}{2}(R - Lc\beta_2') \\ Ls\beta_2' \end{bmatrix} \quad (14)$$

$$^{O_1}Q_3 = \begin{bmatrix} -\frac{1}{2}(R - Lc\beta_3') \\ \frac{\sqrt{3}}{2}(R - Lc\beta_3') \\ Ls\beta_3' \end{bmatrix} \quad (15)$$

The vectors are further determined as:

$$\boldsymbol{Q_1Q_2} = \begin{bmatrix} -\frac{1}{2}(3R - 2Lc\beta_1' - Lc\beta_3') \\ -\frac{\sqrt{3}}{2}(R - Lc\beta_3') \\ L(s\beta_3' - s\beta_1') \end{bmatrix} \quad (16)$$

$$\boldsymbol{Q_1Q_3} = \begin{bmatrix} -\frac{1}{2}(3R - 2Lc\beta_1' - Lc\beta_3') \\ -\frac{\sqrt{3}}{2}(R - Lc\beta_3') \\ L(s\beta_3' - s\beta_1') \end{bmatrix} \quad (17)$$

The distance from point O_1 to the plane $Q_1Q_2Q_3$ is:

$$d_2 = \frac{|-(m_2(R - Lc\beta_1') + p_2 Ls\beta_1')|}{\sqrt{m_2{}^2 + k_2{}^2 + p_2{}^2}} \quad (18)$$

Therefore, the solution parameters are:

$$l_2 = |O_1O_2| = 2d_2 = \frac{2|-(m_2(R - Lc\beta_1') + p_2 Ls\beta_1')|}{\sqrt{m_2{}^2 + k_2{}^2 + p_2{}^2}} \quad (19)$$

$$\delta_2 = \arctan\frac{k_2}{m_2} \quad (20)$$

$$\theta_2 = 2\arctan\frac{\sqrt{m_2{}^2 + k_2{}^2}}{p_2} \quad (21)$$

Where m_2, p_2, k_2 are all functions of β_i' and can be indirectly converted into functions of β_i.

The vector $\boldsymbol{OO_1}$ can be expressed as:

$$\boldsymbol{OO_1} = (l_1 \sin\varphi_1 \cos\delta_1, l_1 \sin\varphi_1 \sin\delta_1, l_1 \cos\varphi_1) \quad (22)$$

The vector $\boldsymbol{O_1O_2}$ in the O_1 coordinate system can be expressed as:

$$^{O_1}\boldsymbol{O_1O_2} = (l_2 \sin\varphi_2 \cos\delta_2, l_2 \sin\varphi_2 \sin\delta_2, l_2 \cos\varphi_2) \quad (23)$$

The vector $\boldsymbol{OO_2}$ can be expressed as:

$$\boldsymbol{OO_2} = \boldsymbol{OO_1} + {}^{O}\boldsymbol{R}_{O_1}\boldsymbol{O_1O_2} = l_x, l_y, l_z \quad (24)$$

The distance between the centers of the moving platform and the static platform is:

$$L = \sqrt{l_x^2 + l_y^2 + l_z^2} \quad (25)$$

The direct kinematic analysis of the mechanism is validated through simulation, with the link length $L = 0.07848m$ and platform radius $r = 0.04497m$ measured. The motion trajectory is described by the following equation:

International Journal of Engineering Research & Technology (IJERT)
ISSN: 2278-0181
Vol. 13 Issue 08, August-2024

$$p(t)=\begin{cases}-0.8t^2+8t+95 & 0\le t\le 5\\ 0 & 5<t\le 15\end{cases}$$

（26）

$$\theta(t)=\begin{cases}0 & 0\le t\le 5\\ -0.32t^3+7.4t^2-48t+100 & 5<t\le 10\\ 0 & 10<t\le 15\end{cases}$$

（27）

$$\phi(t)=\begin{cases}0 & 0\le t\le 5\\ 0 & 5<t\le 10\\ 3.6t^2-72t+360 & 10<t\le 15\end{cases}$$

（28）

The motion trajectory of the center point of the moving platform is shown in Figure 3, and its positional solution is shown in Figure 4.

Figure 3 Motion Trajectory

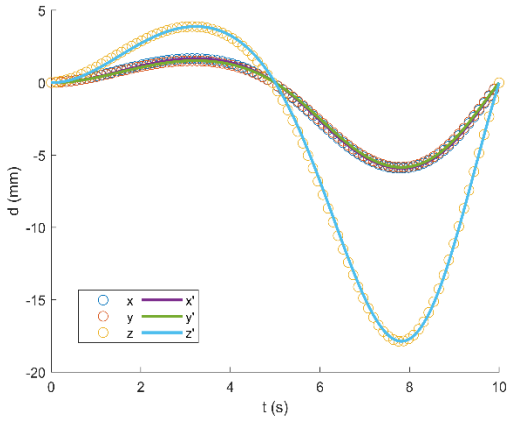

Figure 4 Position Solution

4. SPEED ANALYSIS

According to the differential mapping in the finite instantaneous spiral theory, the velocity model can be solved by differential equations

$$\boldsymbol{S}_{t,i}=\dot{\boldsymbol{S}}_{f,\mathrm{PM}}=\boldsymbol{S}_{t,1}\bigcap\boldsymbol{S}_{t,2}\bigcap\boldsymbol{S}_{t,3}\quad（29）$$

$$\sum_{k=1}^{5}\boldsymbol{S}_{t,i,k}=\sum_{k=1}^{5}\dot{\theta}_{i,k}\hat{\boldsymbol{S}}_{t,i,k},i=1,2,3\quad（30）$$

In the structure, the velocity model of the moving platform is:

$$\boldsymbol{S}_{t,i}=\dot{\theta}_{11,i}\begin{pmatrix}\boldsymbol{s}_{1,i}\\ \boldsymbol{r}_{11,i}\times\boldsymbol{s}_{11,i}\end{pmatrix}+\dot{\theta}_{12,i}\boldsymbol{T}\begin{pmatrix}\boldsymbol{s}_{1,i}\\ \boldsymbol{r}_{12,i}\times\boldsymbol{s}_{1,i}\end{pmatrix}\quad（31）$$

In the structure, the velocity model of the moving platform is:

$$\boldsymbol{S}_{t,i}=\sum_{k=1}^{4}\dot{\boldsymbol{q}}_{i,k}\hat{\boldsymbol{S}}_{t,i,k},i=1,3\quad（32）$$

where $\hat{\boldsymbol{S}}_{t,i,k}$ is the unit instantaneous motion i axis of the first joint in the first rod, and $S_{i,k}$ as its unit direction vector, is its intensity.

$$\mathbf{S}_{w,i}=f_{a,i,3}\hat{\mathbf{S}}_{wa,i,3}+\sum_{kc=1}^{2}f_{c,i,kc}\hat{\mathbf{S}}_{wc,i,kc},i=1,3\quad（33）$$

$$\hat{\mathbf{S}}_{wa,i,3}=\begin{pmatrix}\boldsymbol{r}_{i,3}\times\boldsymbol{s}_{i,3}\\ \boldsymbol{s}_{i,3}\end{pmatrix},\hat{\mathbf{S}}_{wc,i,1}=\begin{pmatrix}\boldsymbol{r}_{i,2}\times\boldsymbol{s}_{i,2}\\ \boldsymbol{s}_{i,2}\end{pmatrix},\hat{\boldsymbol{S}}_{wc,i,2}=\begin{pmatrix}\boldsymbol{s}_{i,2}\times\boldsymbol{s}_{i,1}\\ \mathbf{0}\end{pmatrix}\quad（34）$$

$$\hat{\mathbf{S}}_{wa,i,3}=\begin{pmatrix}\boldsymbol{r}_{i,3}\times\boldsymbol{s}_{i,3}\\ \boldsymbol{s}_{i,3}\end{pmatrix},\hat{\mathbf{S}}_{wc,i,1}=\begin{pmatrix}\boldsymbol{r}_{i,2}\times\boldsymbol{s}_{i,2}\\ \boldsymbol{s}_{i,2}\end{pmatrix},\hat{\boldsymbol{S}}_{wc,i,2}=\begin{pmatrix}\boldsymbol{s}_{i,2}\times\boldsymbol{s}_{i,1}\\ \mathbf{0}\end{pmatrix}$$

（34）

$$\boldsymbol{J}_w\dot{S}_t=\boldsymbol{J}_q\dot{\boldsymbol{q}}\quad（35）$$

$$\boldsymbol{J}_w=\begin{bmatrix}\boldsymbol{J}_{wa}\\ \boldsymbol{J}_{wc}\end{bmatrix},\boldsymbol{J}_q=\begin{bmatrix}\boldsymbol{J}_{qa} & \boldsymbol{o}\end{bmatrix},\dot{\boldsymbol{q}}=\begin{bmatrix}\dot{\boldsymbol{q}}_a\\ \mathbf{0}_{3\times1}\end{bmatrix},\dot{\boldsymbol{q}}_a=\dot{i}_{1,3}\begin{bmatrix}\dot{t}_{1,3} & \dot{t}_{2,4} & \dot{t}_{3,3}\end{bmatrix}^{\mathrm{T}}$$

（36）

$$\boldsymbol{J}_{wa}=\begin{bmatrix}\hat{\boldsymbol{S}}_{wa,1,3} & \hat{\boldsymbol{S}}_{wa,2,4} & \hat{\boldsymbol{S}}_{wa,3,3}\end{bmatrix}^{\mathrm{T}},\boldsymbol{J}_{wc}=\begin{bmatrix}\hat{\boldsymbol{S}}_{wc,1,1} & \hat{\boldsymbol{S}}_{wc,2,1} & \hat{\boldsymbol{S}}_{wc,3,1}\end{bmatrix}^{\mathrm{T}}$$

（37）

International Journal of Engineering Research & Technology (IJERT)
ISSN: 2278-0181
Vol. 13 Issue 08, August-2024

$$\boldsymbol{J}_q = \begin{bmatrix} \hat{\boldsymbol{S}}^{\mathrm{T}}_{wa,1,3}\hat{\boldsymbol{S}}_{t,1,3} & & \\ & \hat{\boldsymbol{S}}^{\mathrm{T}}_{wa,2,4}\hat{\boldsymbol{S}}_{t,2,4} & \\ & & \hat{\boldsymbol{S}}^{\mathrm{T}}_{wa,3,3}\hat{\boldsymbol{S}}_{t,3,3} \\ & & \boldsymbol{0} \end{bmatrix} \tag{38}$$

5 CONCLUSION

(1) A configuration idea of connecting the parallel mechanism in series in the form of a mechanism unit is proposed, and the multi-level coupling connection mechanism with the 3-RSR parallel mechanism as the structural unit is proposed, and the motion space is improved after two superimpositions. This kind of mechanism has both a large working space for a series mechanism and a dynamic performance of a parallel mechanism.

(2) The position analysis of the single-layer 3-RSR mechanism is carried out by using the allocation principle, and the velocity is solved by using the finite instantaneous spiral theory, and the simulation verification is carried out, which lays a foundation for the research of multi-level coupling and linking mechanism.In terms of research content, the neural network model established in this study calculates the mean square error (MSE) to verify the model's reliability. The optimal parameters are found using the Bayesian optimization algorithm. Finally, the reliability of the model is verified through path planning analysis.

(3) The configuration proposed in this paper is obviously different from the previous configuration, and also realizes some motion characteristics that the existing parallel mechanism does not have, and uses the finite instantaneous spiral theory to solve the velocity, which has a certain originality, and the feasibility of the coupling idea of multi-stage parallel mechanism is verified by the position and velocity simulation of the 3-RSR mechanism.

REFERENCES

[1] Li M, Cao Z, et al. 3-DOF bionic parallel mechanism design and analysis for a snake-like robot[C]//2016 IEEE International Conference on Robotics & Biomimetics. Harbin: IEEE, 2016: 25-30.

[2] VERL A, VALENTE A, MELKOTE S, et al. Robots in machining[J]. CIRP Annals,2019,68(2):799-822.

[3] BU Y, LIAO W, TIAN W, et al. Stiffness analysis and optimization in robotic drilling application[J]. Precision Engineering,2017(1):388-400

[4] S. L. Li, Y. W. Wang, and Z. Wu, "Design of a four-degree-of-freedom concrete spraying device with tandem and hybrid," Sci. Technol. Innov., vol. 209, no. 17, pp. 63–65, 2022.

[5] Li Z, Feiling J, et al. A Novel Tele-Operated Flexible Robot Targeted for Minimally Invasive Robotic Surgery[J]. Engineering, 2015, 1(1): 073-078.

[6] S. L. Li, Y. W. Wang, and Z. Wu, "Design of a four-degree-of-freedom concrete spraying device with tandem and hybrid," Sci. Technol. Innov., vol. 209, no. 17, pp. 63–65, 2022.

[7] M. H. Wang and M. X. Wang, "Dynamic modeling and performance evaluation of a new five-degree-of-freedom hybrid robot," CJME, vol. 59, no. 59, pp. 1–13, 2023.

[8] C. D. Zeng, H. P. Ai, and L. Chen, "Force/pose impedance control for space manipulator orbit insertion and extraction," CJME, vol. 58, no. 3, pp. 84–94, 2022.

[9] J. Peng, H. Wu, T. Liu, and Y. Han, "Workspace, stiffness analysis and design optimization of coupled active-passive multilink cable-driven space robots for on-orbit services," Chin. J. Aeronaut., vol. 36, no. 2, pp. 402–416, Feb. 2023.

[10]H. Liu, D. Y. Liu, and Z. N. Jiang, "Space manipulator technology: Review and prospect," Acta Aeronauticaet Astronautica Sinica, vol. 42, no. 1, pp. 33–46, 2021.

[11]Q.X. Jia, P. Ye, H.-X. Sun, and J.-Z. Song, "Kinematics of a trinal-branch space robotic manipulator with redundancy," Chin. J. Aeronaut., vol. 18, no. 4, pp. 378–384, Nov. 2005.

[12] T.-L. Yang, A.-X. Liu, Q. Jin, Y.-F. Luo, H.-P. Shen, and L.-B. Hang, "Position and orientation characteristic equation for topological design of robot mechanisms," J. Mech. Des., vol. 131, no. 2, pp. 021001-1–021001-17, Feb. 2009.

[13]T.-L. Yang, A.-X. Liu, H.-P. Shen, Y.-F. Luo, L.-B. Hang, and Z.-X. Shi, "On the correctness and strictness of the position and orientation characteristic equation for topological structure design of robot mechanisms," J. Mech. Robot., vol. 5, no. 2, pp. 021009-1–021009-18, May 2013.

International Journal of Engineering Research & Technology (IJERT)
ISSN: 2278-0181
Vol. 13 Issue 08, August-2024

[14] Q. Li and J. M. Herve, "Type synthesis of 3-DOF RPR-equivalent parallel mechanisms," IEEE Trans. Robot., vol. 30, no. 6, pp. 1333–1343, Dec. 2014.

[15]J. T. Li, H. B. Xu, and X. Y. Zhai, "Research on the architecture of in-orbit robot service system based on space station platform," Robot Technique Appl., vol. 200, no. 2, pp. 45–48, 2021.

[16] Y. Y. Wang, C. W. Hu, Z. X. Tang, and S. Gao, "Key technologies development of the space station manipulator system," Spacecraft Eng., vol. 31, no. 6, pp. 147–155, 2022.